GEOPHYSICS, VOL. 59, NO. 7 (JULY 1994); P. 1072-1082, 15 FIGS.

Electrical resistivity measurement through metal casing

Clifford J. Schenkel* and H. Frank Morrison*

ABSTRACT

Methods using dc electrical arrays to measure formation resistivity through casing have relied on approximate forms for the current and potential distributions to derive a simple relationship between the formation resistivity and the transverse resistance calculated from measurements of the potential and its second derivative inside the casing. We have derived a numerical solution for the potentials and their derivatives to examine the accuracy of the approximate forms for casing of finite-length, annular zones of varying radius, and for vertical discontinuities such as layers or abrupt changes in annular zone radius. For typical conductivity contrasts between the casing and formation, the approximate relationships may be off by as much as 60 percent for long casing and may show variations of 20 to 30 percent as the electrode array moves along the casing. In principle an iterative scheme could be devised to correct the readings if high accuracy was required. The numerical results show that to first order the current flow from the casing is radial, and that all the analytic expressions based on this assumption for evaluating layer resolution and the effects of annular layers are valid. An interesting byproduct of this study has been the discovery that the distortion of the potentials in a nearby well by an annular disk (e.g., an injected steam zone) surrounding the current injection well is greater if the injection well is cased. Crosswell resistivity surveys appear feasible if one of the wells is cased.

INTRODUCTION

Recent studies by Kaufman (1990) and a series of patents by Kaufman (1989), Vail (1989a, b), and Gard et al. (1989) have demonstrated the practical feasibility of measuring formation resistivity with direct current (dc) electrical devices that operate within a cased well.

The principles of such measurements are straightforward. The current from a point source within a cased hole flows away by two major paths; along the casing and by "leakage" from the casing into the formation. The amount flowing along the casing is determined primarily by the casing conductance S_c, and the amount leaking into the formation is controlled by a transverse resistance T, which is basically the resistance offered to current leaving the metal casing and flowing radially into the formation. This resistance is also referred to as the contact resistance, and it in turn is proportional to the formation resistivity ρ_f.

The practical field embodiment of this idea by Vail et al. (1993) uses a multielectrode configuration that first uses a closely coupled array to determine the casing conductance and then a second array comprised of some of the electrodes of the first plus an electrode at "infinity" to measure the drop in electric field in the casing to determine the leakage current and hence T. This device is called the Through-Casing Resistivity Tool (TCRT™), and with several technical modifications to correct for second order effects, it has been used with excellent results (Vail et al., 1993).

While it has been demonstrated that in infinite pipes in infinite media the transverse resistance can be measured and that it is proportional to the formation resistivity, it is not clear what the relationship is between these two parameters in practical situations of finite-casing length, variable invasion zones, or layered formations.

Kaufman's fundamental paper (Kaufman, 1990) presented a solution for Poisson's equation for a point source of current I_0 on the axis of an infinitely long borehole of a

Manuscript received by the Editor January 31, 1992; revised manuscript received January 17, 1994.
*Formerly University of California at Berkeley; presently Lawrence Livermore National Laboratory, P.O. Box 808, L-156, Livermore, CA 94550.
‡Engineering Geoscience, University of California at Berkeley, 414 Hearst Mining Building, Berkeley, CA 94720.

radius a in a uniform medium. The borehole was either filled with uniform high conductivity material (a solid conducting cylinder of conductivity a,) or cased with a conducting metal pipe of radius a, thickness Δa and conductivity σ_c. In the former, the borehole "conductance" S_c is given by $\pi a^2 \sigma_c$ in the latter by $S_c = 2\pi a \Delta a \sigma_c$. These "conductances," which actually have the units of S l m as defined by Kaufman are the reciprocals of the unit length longitudinal resistance of the casing. The final expressions for the potential field (ϕ) and field derivatives along the casing involve straightforward integrals of modified Bessel functions that are not simple to interpret in terms of the physics of solutions. Plotting the second vertical derivative of the potential (ϕ''), it is found that there is a region where ϕ'' is approximately constant. Kaufman found that the electric field E_z in this intermediate zone can be described approximately by

$$\frac{\partial \phi}{\partial z} = E_z \approx \frac{I_0}{2S_c} e^{-z/\sqrt{\rho_f S_c}} \tag{1}$$

and correspondingly

$$4'' = \frac{\partial^2 \phi}{\partial z^2} \approx \frac{I_0}{2S_c} \frac{1}{\sqrt{\rho_f S_c}} e^{-z/\sqrt{\rho_f S_c}}. \tag{2}$$

Schenkel(l991) termed $\sqrt{\rho_f S_c}$ the conduction length 6, and it describes the distance over which l/e of the injected current leaks out of the pipe into the formation. Kaufman (1990) noted further that in the intermediate zone, if $z < \delta$ then the second derivative of the potential is almost constant and equal to

$$4'' \approx \frac{I_0}{2S_c^{3/2}} \sqrt{\sigma_f}. \tag{3}$$

This equation basically solves the problem of logging through casing. With an apparatus designed to operate in the intermediate range, measurements of the second derivative of the potential along the borehole, the current, and a knowledge of S_c (from another measurement to be made independently), allow one to derive the formation conductivity. Kaufman (1990) then used the simple behavior of the potential derivatives in the intermediate zone to bring in the analogy of a transmission line to represent the solution.

In his transmission line analogy the physics of the solution is more easily seen. In an insulating formation the voltage drop in a segment is given simply by Ohm's law. If the surrounding formation is not insulating, then current will leave the segment via some resistance and with a driving voltage equal to the mean voltage on the segment. The leakage current will just equal the drop in axial current along the segment. Kaufman (1990) derives this relationship using a quantity T, the inverse of the unit length leakage conductance (unit of $\Omega \cdot$ m), to describe the resistance to current flow into the formation. With this quantity he finds the governing equation to be

$$\frac{\partial^2 \phi}{\partial z^2} = \frac{1}{TS,} \; 4_1 \tag{4}$$

This equation itself is extremely useful since it permits the recovery of T (which we will see is related to ρ_f) from measurements of potentials only.

From the solutions to the transmission line equation, Kaufman derives the expression for E_z, viz.

$$E_z = \frac{I_0}{2S_c} e^{-z/\sqrt{TS_c}} \tag{5}$$

and

$$4^{\mathbb{I}} = \frac{\partial^2 \phi}{\partial z^2} = \frac{I_0}{2S_c} \frac{1}{\sqrt{TS_c}} e^{-z/\sqrt{TS_c}} \; 1 \tag{6}$$

We see quite clearly the direct relationship to the early solution of equation (2) and find that T is in fact equal to ρ_f.

To test the accuracy of the approximations, we first calculated T from equation (4) using the values of 4 and 4" from the analytic solution for an infinitely long solid cylinder that was derived by Kaufman. We used the solid pipe for simplicity, and the results shown in Figure 1 are for pipes of varying contrast (σ_c/σ_f) with the formation. The ordinate is the ratio of T calculated from equation (4) to the actual formation resistivity ρ_f, and the abscissa is the ratio of the distance from the current source to the measuring point normalized by the diameter of the pipe *(z/a).* There is a limited range over which T equals ρ_f. For all large contrasts, T is consistently larger than ρ_f in the intermediate zone, and for the realistic situation of steel pipe in a formation of 100 Ω l m resistivity the error may be greater than 60 percent.

As the contrast increases even more, for example as the casing approaches prefect conductivity, T will actually go to infinity as clearly pointed out by Kaufman [1990, equation 51]. In such a situation, an infinite pipe of uniform potential and uniform radial current is unrealizable. The finite conductance and finite length always produce a longitudinal component of leakage current and avoids infinite values for T.

The simple formula for estimating ρ_f depends on the assumption that the current flow into the formation is purely radial, and since this is only an approximation in the infinite pipe, we decided to investigate the exact form of the solutions for finite-length pipes, for pipes intersecting layers, and for cylindrical annuli (disks) around the casing. We anticipated that the conduction length is so great for typical casing and formation resistivity that infinite pipe is rarely a good assumption (especially as a logging tool approaches the

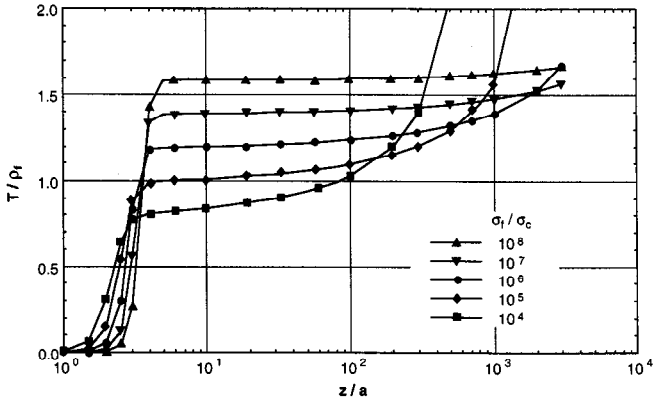

FIG. 1. Ratio of the transverse resistance to formation resistivity (T/ρ_f) for different conductivity ratios calculated for the infinite solid cylinder.

end), that a layer might easily perturb the current vector well before the tool enters the layer, and that variation in an annular layer (an invaded zone) might also perturb the current vectors enough to seriously affect estimates of the formation resistivity.

In this study, we develop a numerical solution for a finite-length, fluid-filled casing in a layered and radially inhomogeneous medium. This solution was verified by comparing the numerically calculated potentials for a long solid cylinder in a half-space to those obtained analytically for a semi-infinite cylinder. We study the problem using an electrode array similar to the early logging tool of Vail (1989a). In this configuration, two current and three potential electrodes, moved down the well, are in contact with the casing and have fixed separations. We present the results in terms of T as defined in equation (4) because this is the approach suggested by Kaufman (1990), and it illustrates the fundamental nature of the response that can be expected with any such array in nonuniform media.

INTEGRAL EQUATION FORMULATION

The surface integral equation technique (Eloranta, 1986), used to calculate the potentials, models a borehole fluid, casing, and layer as inhomogeneities in a background half-space. It is assumed that the sources are on the vertical z-axis and the casing and inhomogeneities have axial symmetry with z so that the cylindrical coordinate system can be used. Because of axial symmetry, the field can be described by its radial (x) and vertical (z) components.

Application of Green's theorem to Poisson's equation and the boundary conditions gives a Fredholm integral equation of the second kind for the potential function 6(r):

$$\phi(\mathbf{r}) = \phi_0(\mathbf{r}) + \left[1 - \frac{\sigma_1}{\sigma_0}\right] \int_S \phi(\mathbf{r}')\nabla' g(\mathbf{r}, \mathbf{r}')\ \hat{\mathbf{n}}(\mathbf{r}')\ ds', \tag{7}$$

where σ_0 is the background conductivity, σ_1 is the disturbing body conductivity, and $\mathbf{r}$, $\mathbf{r}'$, and $\hat{\mathbf{n}}$ are the field point, source density point, and outward unit surface normal vector on S, respectively.

The axisymmetric half-space Green's function used for this problem is (see, e.g., Schenkel and Morrison, 1990):

$$g(\mathbf{r}, \mathbf{r}') = \frac{1}{4\pi} \int_0^\infty J_0(\lambda x) J_0(\lambda x') \times [e^{-\lambda|z - z'|} + e^{-\lambda(z + z')}]\, d\lambda, \tag{8}$$

where $J_0(y)$ is the Bessel function of order zero, and the primed and unprimed values are the locations of the source and field points, respectively.

The integral equation (7) is solved by expanding the unknown function into a series of N piecewise constant basis functions. The Dirac delta weighting functions are then used to satisfy equation (7) at each of the N discrete points on the region of interest. The integral over the region is approximated as a summation of integrals over the subsections. Thus, equation (7) can be approximated by

$$\phi(\mathbf{r}_m) = \phi_0(\mathbf{r}_m) + \left[1 - \frac{\sigma_1}{\sigma_0}\right] \sum_{n=1}^{N} K(\mathbf{r}_m, \mathbf{r}'_n)\phi(\mathbf{r}'_n), \tag{9}$$

where

$$K(\mathbf{r}_m, \mathbf{r}'_n) = \int_{S_n} \nabla' g(\mathbf{r}_m, \mathbf{r}'_n) \cdot \hat{\mathbf{n}}(\mathbf{r}'_n)\ ds' = n(\mathbf{r}'_n) \int_{S_n} \frac{\partial}{\partial n'} g(\mathbf{r}_m, \mathbf{r}'_n)\ ds', \tag{10}$$

and n is the directional cosine for the nth subsection. This matrix equation can be solved to determine the unknown potential functions. Once the surface potentials are found, equation (9) is used to calculate the potential at the field point.

For the casing, or any other annular-shaped objects, there are two components, i.e., radial and vertical, to the surface integral. Equation (10) can now be expressed as

$$K(\mathbf{r}, \mathbf{r}') = n_z K_z(\mathbf{r}, \mathbf{r}') + n_x K_x(\mathbf{r}, \mathbf{r}'). \tag{11}$$

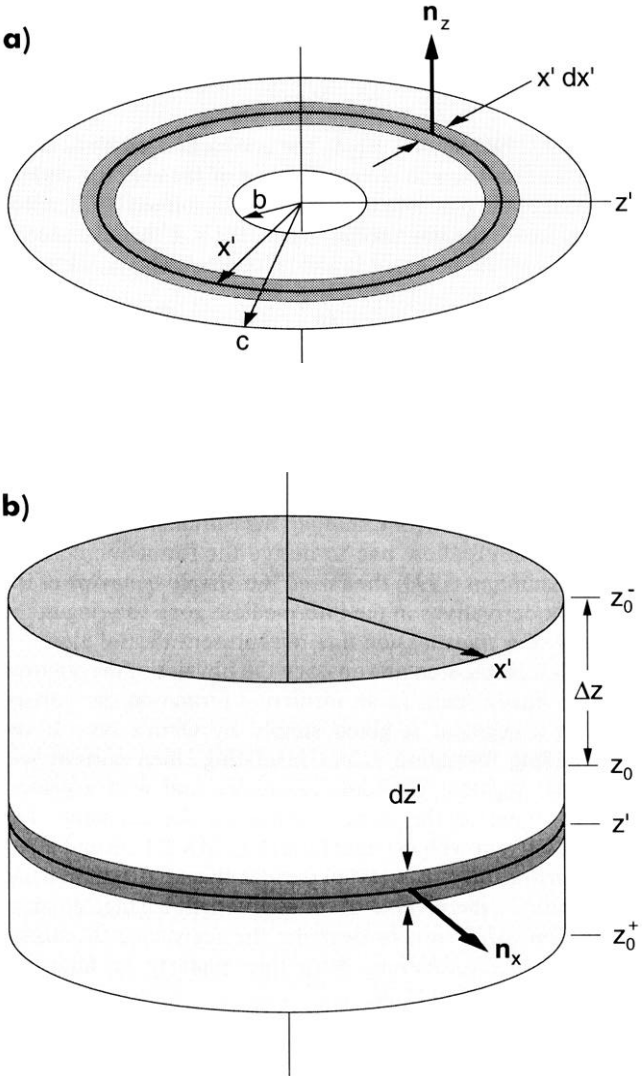

FIG. 2. The two surface elements associated with an annular segment. The horizontal disk (a) defines the top and bottom annular surfaces. The vertical cylindrical shell (b) represents the inner and outer walls of the annulus.

Figure 2 illustrates the two surface types associated with an annular object. The K_z -integral defines the flat horizontal ring surface (disk) of the top and bottom parts of the annular object. The K_x -integral describes the vertical cylindrical shell of the inner and outer walls of the annulus. For brevity, only the K-integrals, which are solved in Schenkel (1991), are given here:

$$K_z = \tfrac{1}{2}\{\text{sgn}\,(z - z')[F(b, x, |z - z'|) - F(c, x, |z - z'|)] - [F(b, x, z + z') - F(c, x, z + z')]\}, \quad (12a)$$

and

$$K_x = \frac{1}{2}\left\{\begin{bmatrix}+1\\-1\\+1\end{bmatrix}F(x', x, |z - z_0^-|) + \begin{bmatrix}-1\\+1\\-1\end{bmatrix}F(x', x, |z - z_0^+|) + F(x', x, z + z_0^+) - F(x', x, z + z_0^-)\right\} - \begin{bmatrix}0\\0\\1\end{bmatrix}F(x', x, 0) \quad \text{for} \begin{bmatrix} z \le z_0^- \\ z \ge z_0^+ \\ z_0^- < z < z_0^+ \end{bmatrix}, \quad (12b)$$

where $z_0^+ = z_0 + \Delta z$ and $z_0^- = z_0 - \Delta z$.

The function $F(u, v, w)$ is (Luke, 1962):

$$F(u, v, w) = u \int_0^\infty J_1(\lambda u) J_0(\lambda v) e^{-\lambda w}\, d\lambda$$

$$\begin{cases} 1 - \dfrac{wkK(k)}{2\pi(uv)^{1/2}} - \dfrac{1}{2}\Lambda_0(\psi, k), & u > v \\ \dfrac{1}{2} - \dfrac{wkK(k)}{2\pi u}, & u = v, \\ 0 - \dfrac{wkK(k)}{2\pi(uv)^{1/2}} + \dfrac{1}{2}\Lambda_0(\psi, k), & u < v, \end{cases} \quad (13a)$$

where $\Lambda_0(\psi, k)$ is the Heuman lambda function,

$$k = \left[\frac{4uv}{w^2 + (u + v)^2}\right]^{1/2}$$

and

$$\sin\psi = \left[\frac{w^2}{w^2 + (u - v)^2}\right]^{1/2}. \quad (13b)$$

The numerical accuracy of the algorithm has been checked against the analytic solution for a semi-infinite solid cylinder. The semi-infinite solution was produced by applying the method of images to the vertical infinite cylinder solution. Figure 3 is a plot of the potentials versus the normalized depth (z/a) for various conductivity ratios (σ_c/σ_f). The solid lines are the analytic solutions and the symbols are the corresponding numerical solution. Each numerical solution represents a particular model with a given length, L, of the solid cylinder and conduction length, $\delta = \sqrt{\rho_f S_c}$. Since the cpu time to invert the matrix is proportional to the matrix size cubed, we used lengths only long enough to approximate the infinite length cylinder.

The potentials show an agreement as long as the length of the cylinder is over four times the conduction length. When the length of the cylinder is less than this value, the numerical solutions are greater than those calculated from the analytic solution. We could not approximate the "infinite" cylinder for such conduction lengths since the number of cells exceeded our computer memory. However, the potentials did converge as the cell size decreased for a given cylinder length. When the cylinder is long enough to appear infinite then the second derivative was accurate. The cell size Az must be much smaller than the electrode separation δz to permit numerical accuracy of the second derivative. The size and number of cells are dependent on the conduction length of the cylinder and the geometry of the array. However, a cell size of $Az < \delta z/10$ is sufficient for less than 5 percent errors in approximating the second derivative.

NUMERICAL RESULTS

For this study, we have used a simple electrode array and measuring scheme similar to that described in the patent of Vail (1989a). Two independent sets of measurements from a three-point electrode array (Figure 4) are required to calculate the casing conductance, and then the transverse resistance is calculated from the potential and its second derivative.

For the first array configuration (the calibration or compensation state), the current I is applied at the source electrodes A and B which are in close proximity to the potential electrodes M, N, and M'. Because of the large contrast in conductivities between the casing and adjacent formation, essentially all of the current will flow within the casing. Thus the voltages V_1 and V_2 measured across their respective electrode pairs, MN and NM', will reflect the conductance of the casing between the electrode pairs. By measuring V_1 and V_2 separately and knowing the current strength, the conductance for each section can be estimated from Ohm's law:

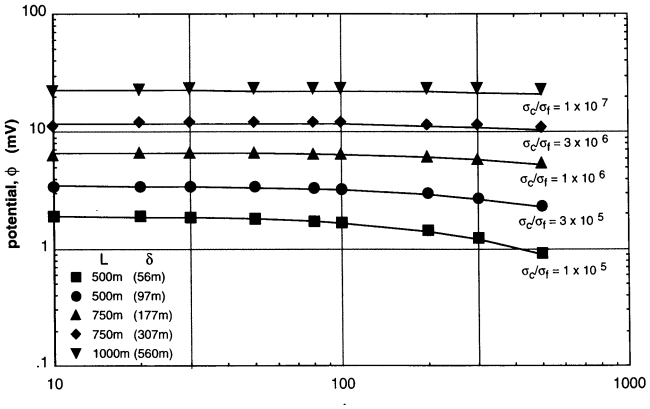

FIG. 3. The potentials on the borehole axis for different casing conductivity (a,) to formation conductivity (a) ratios. The solid lines and symbols are calculated from the infinite solid cylinder and integral equation, respectively.

$$S_{ci} = \frac{I\Delta z}{V_i} \quad \text{(for } i = 1, 2\text{).} \tag{14}$$

This expression assumes no current leakage into the formation. There may be some leakage if the potential electrodes are located "too far" from the current source in a highly conductive formation. In practice, the spacings are on the order of meters. The numerical calculation of S_c using equation (14) agrees with the known values to better than 1 percent.

With the second electrode configuration (the measurement state), the current electrode B is moved to a remote position (infinity in theory). Now the current must not only flow in the casing but also through the formation. The measured voltages V_1 and V_2, as well as the potential U_N, will reflect both the casing and formation resistivities. By subtracting the two voltages, an approximation of the second derivative is obtained. With the estimate of the casing conductance and the second derivative, the transverse resistance *T* is calculated from the discrete form of equation (4).

Casing effects

We first studied the effects of radius and length of the casing and the position of the measurement array within the casing on T, the transverse resistance defined above. We used a casing of 10^{-6} Ω · m with length *L*, outside diameter OD, and thickness t, embedded in a homogeneous half-space (See Figure 5a). For this analysis, the separation between the current and center potential electrode AN is 2.8 m, while the potential electrode spacing MN = NM' is 1.4 m.

Figure 5b shows T for a 100 m casing with a variety of common thicknesses and diameters in a 10 Ω · m medium. Variations in casing thickness resulted in a change of *T* of less than 1 percent. However, increases in casing diameter decrease *T* as predicted from equation (4) and produced 5-10 percent variations. The effects of the casing length are dramatic. We used a 0.2286 m (9") OD, 0.0127-m (l/2-inch) thick casing, several casing lengths, and variable host formation resistivities of 1, 10, and 100 Ω · m to calculate the values of *T* in Figure 6. When the ratio of the conduction length to casing length S/L is much larger than 0.5 (this occurs in a resistive formation), the casing begins to act like a "short" grounded electrode and *T* is dependent on the length of the casing. When this ratio is much smaller than 0.5, the casing looks infinitely long and T approaches the resistivity of the formation. The plots also show that even for a long casing, *T* is not constant along the length of the casing, but is dependent on the position of the measurement. The value of T slowly decreases with depth near the surface and rapidly decays near the bottom of the casing.

The results suggest that the casing diameter, casing length, and position of the array play a significant role in estimating the formation resistivity and that in general a correction factor should be applied to T. Finding a factor to correct for the geometric parameters is a study by itself and might yield to an

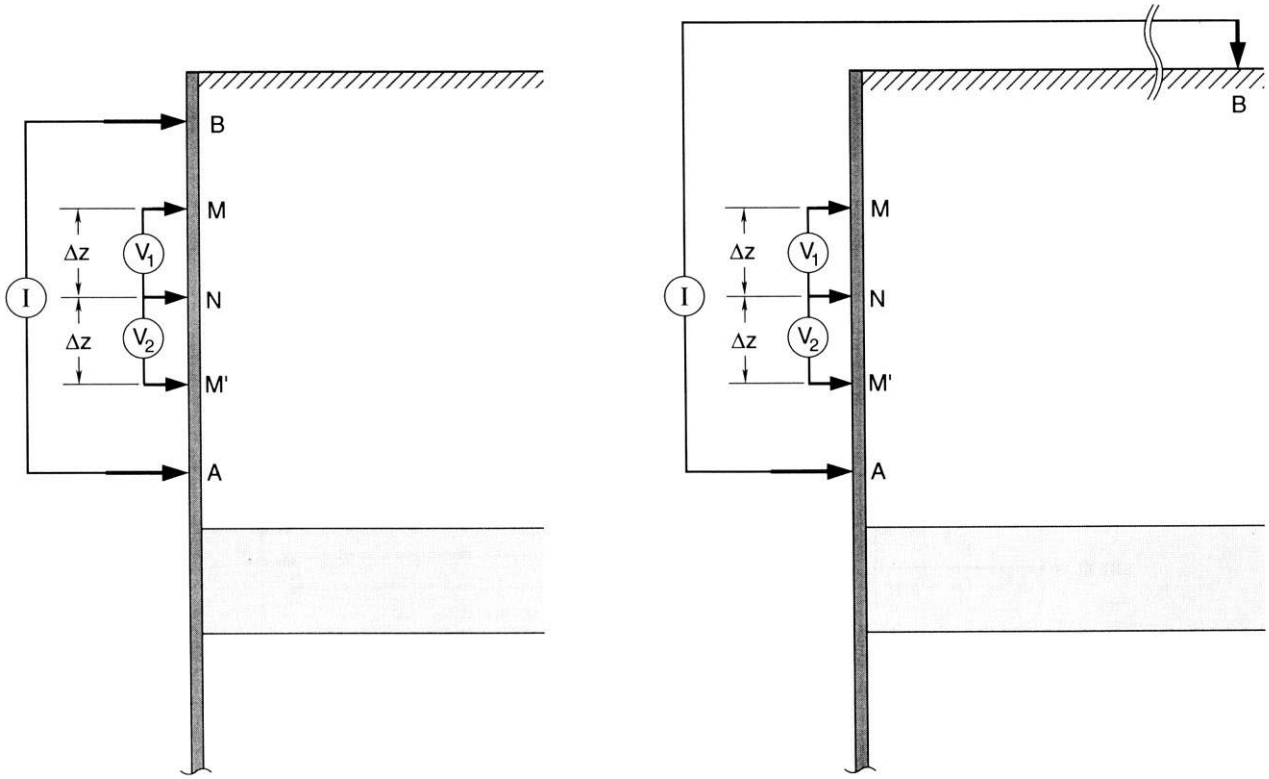

FIG. 4. The two electrode arrays used to calculate the electrical property of the formation. Measurements from the left configuration determine the casing conductance. The right array measures the potential at electrode N and estimates its second derivative from three electrodes: M, N, and M'.

iterative scheme where T is used as a first estimate of the formation resistivity and then corrections are applied given the approximate value of δ/L. At this time, it may be better to note that these parameters must be included in the correction factor to effectively compensate for these casing effects.

Layer response

Figure 7 illustrates the generalized model for investigating the response to layers. A finite-length conductive casing filled with fluid embedded in a three-layer medium is used for this analysis. To simplify computation, a resistivity of 10 $\Omega \cdot m$ is used for the borehole fluid, top layer, and basal half-space. Thus, only the casing and target bed need to be modeled. For this problem, the casing, which is modeled with 1004 segments, has a resistivity of 10^{-6} $\Omega \cdot m$, length of 50 m, inner radius of 0.1 m, and thickness of 1.27 cm. The target bed, which is approximated with 223 cells, is 3 m thick with its top located 22 m below the surface. To approximate a layer of infinite extent, the outer boundary of the layer is placed at 5000 m. The electrode array is the same as that used in the previous results (Figures 5 and 6).

The vertical E-fields, shown in Figure 8, are estimated by dividing the voltage difference between adjacent electrodes by the electrode separation. For this example, the resistivity used for the target layer ranged from 1 $\Omega \cdot m$ to 100 $\Omega \cdot m$. Three general observations can be made from this figure. First, the rate of change of the E-fields is constant for the uniform, 10 $\Omega \cdot m$ medium and has different slopes for each resistivity within the target layer. Second, the change in slope is very small for resistive formations and much larger in the conductive medium. Last, the discontinuity of the curves correspond to the formation boundary. As predicted by Kaufman (1990), even when layers are present the rate of change of the E-field is proportional to the current leakage which is related to the electrical resistivity of the formation. For the conductive layer, the increased rate of voltage drop results from the increased current leakage into the adjacent formation. A resistive formation has the opposite effect, and a decreased rate of change is observed through the layer.

These numerical results for a casing of representative properties indicate that the E-fields must be measured to the order of 10's $\mu V/m$ per unit ampere, and that very small

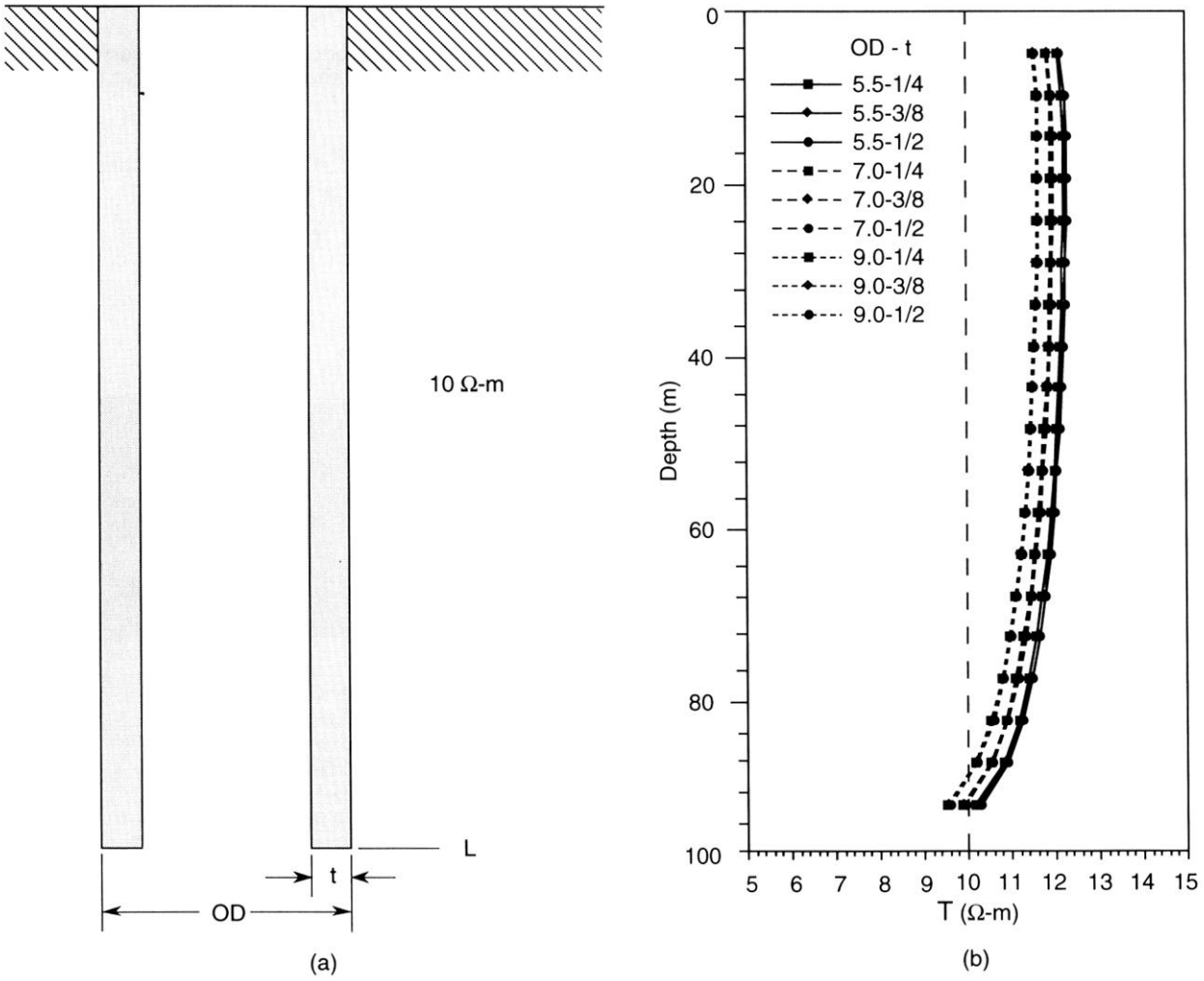

FIG. 5. (a) Generalized model of a casing in a half-space and array configuration and (b) the transverse resistance calculated for several casing thicknesses (t) and outside diameters (OD). The units for t and OD are inches.

changes in the E-field must be distinguishable. For resistive formations, an estimate of the resistivity will be very difficult, if not impossible, since minute **E-field** changes may be lost in the noise level. The rate of change of the E-field for a 100 $\Omega \cdot$ m formation is approximately 0.6 uV/m per meter; whereas, the changes are significantly larger for IO $\Omega \cdot$ m and I $\Omega \cdot$ m formations at 2.2 and 14.0 μV/m per meter, respectively.

A measurement through casing resistivity log with unknown casing conductivity is simulated using the parameters of Figure 7. The separation between current and center potential electrode *AN* was 2.05 m, while the potential electrode spacings MN and NM' were 1.00 m. The numerical results for several resistivities of the target layer are illustrated in Figure 9. The transverse resistance curves,

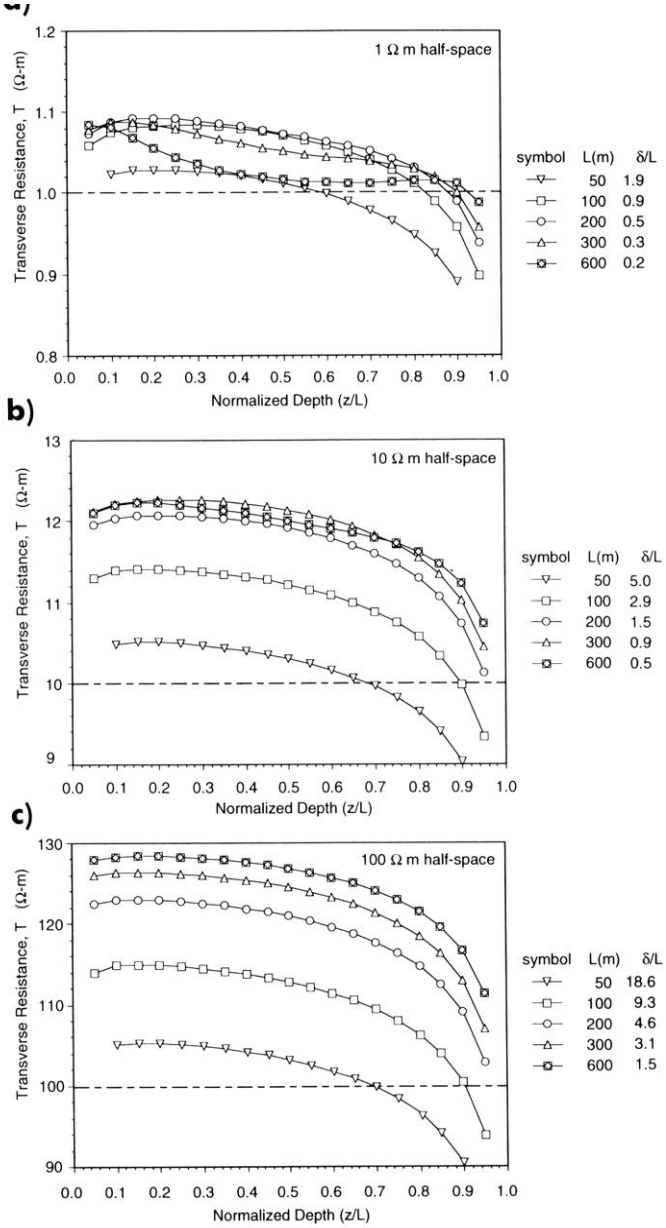

FIG. 6. Transverse resistances calculated for several casing lengths or conduction lengths. The casing has a thickness of 0.0127 m and radius of 0.1016 m and is in a half-space of (a) 1 $\Omega \cdot$ m, (b) 10 $\Omega \cdot$ m, and (c) 100 $\Omega \cdot$ m. Parameter δ is the conduction length ($\sqrt{\rho_f S_c}$).

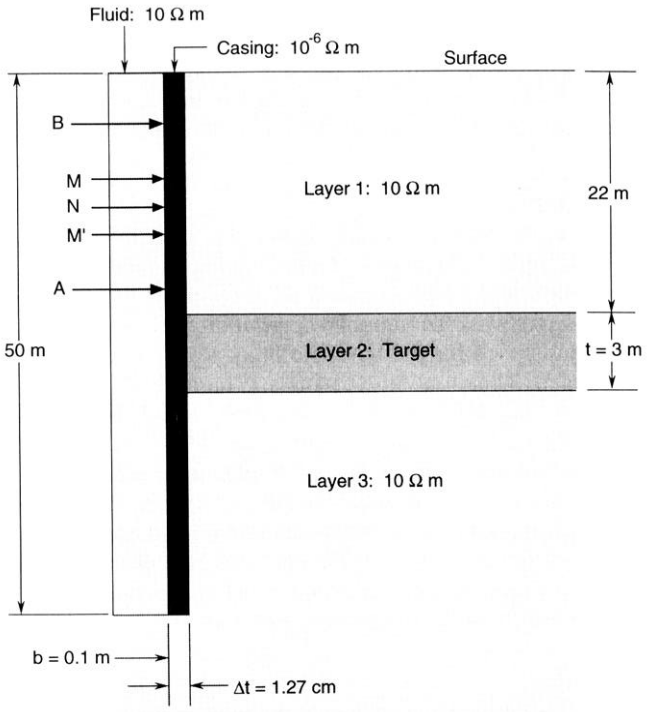

FIG. 7. Generalized model of a fluid-filled casing in a layered medium and the electrode configuration.

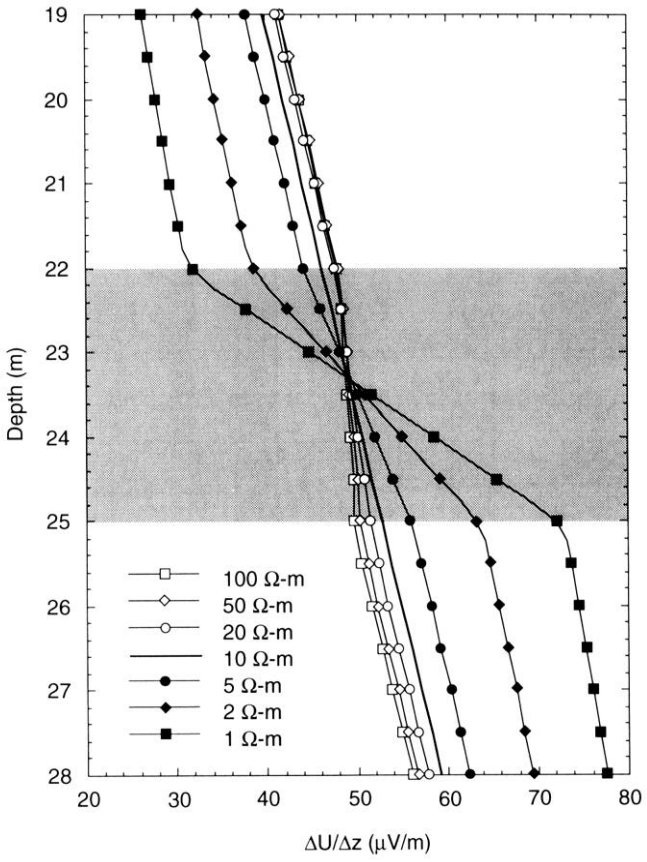

FIG. 8. The vertical electric fields estimated for several resistivities of the target layer (shaded area) and the parameters defined in Figure 7.

calculated by equation (4). respond to the resistivity of the model remarkably well. The transverse resistance value is approximately 10-15 percent greater than the resistivity of the homogeneous (no layer) model as predicted from the earlier discussion relating to the results of Figure I. When the target layer is conductive, the difference between the true resistivity and the transverse resistance is small (≤ 10 percent). This discrepancy increases for increasing layer resistivity; for a 100 $\Omega \cdot m$ layer, the transverse resistance is 20-40 percent greater than the layer resistivity.

The vertical resolution can be examined by measuring the transverse resistance with different electrode spacings at a layer boundary (Figure 10). Several potential electrode separations (Δz) ranging from 0.2 m to 3.0 m were used to illustrate the resolution of the 3 m bed. The parameters shown in Figure 7 were used for this simulation. This figure shows that the resolution of the bed boundary improves as the electrode separation decreases. The distance of resolution is approximately twice the electrode separation ($2\Delta z$) which is needed to estimate the second derivative. This again confirms Kaufman's prediction; basically the very small departures from purely radial current Row do cause *T* to be different from the formation resistivity but are not sufficient to invalidate the argument that boundary resolution is set simply by the electrode separation required to make a satisfactory measurement of the second derivative of the potential

The "full" response of the transverse resistance is not achieved until the electrode spacing is less than one-half the bed thickness ($\Delta z < 1.5$ m). When Az = 1.5 m. only the measurement at the bed center attains the full transverse resistance response. However, one cannot determine if this measurement is the full transverse resistance response of the bed since it could be caused by a thinner and more conductive bed. To remove this ambiguity, several full response measurements must be acquired. Thus. a layer must have a minimum thickness of 2-3 times the electrode separation before the transverse resistance is correctly measured. The irregularities seen in several curves, especially for the smaller electrode spacing, are caused by the numerical instabilities associated with approximating derivatives of fields that vary very slowly. Fewer cells are incorporated in the approximation of the derivative for the smaller separations. In Figure IO, the 0.2-m electrode spacing incorporated *2* cells whereas the case Az = 3.0 m spanned 30 cells.

In summary, it appears that the presence of an interface does not cause any significant increase in the nonradial current Row in the formation as the interface is approached.

Annular layer

For typical resistivity logging methods, increasing the separation of the electrodes increases the radius of investigation. Since the TCRT'" employs only radial current flow,

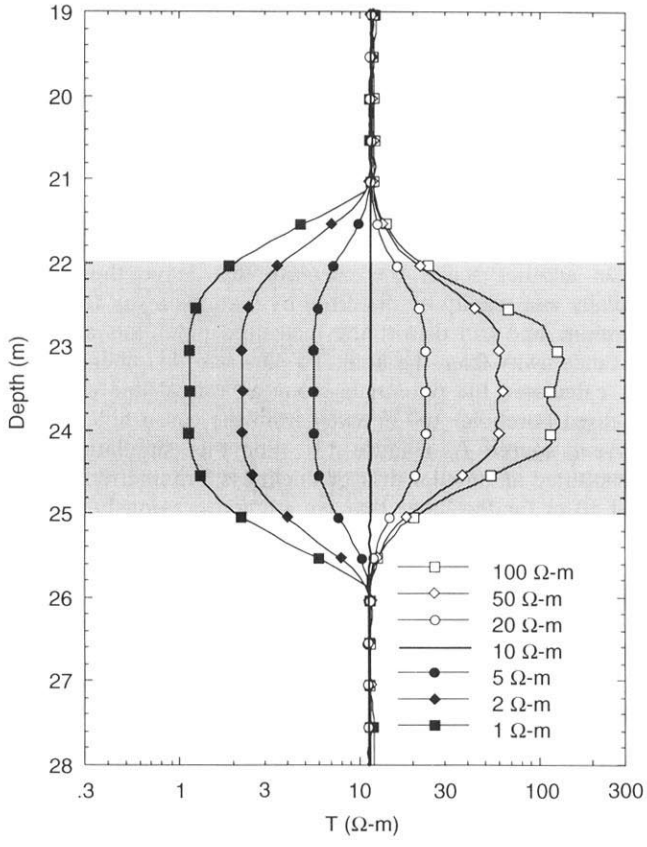

FIG. 9. The transverse resistance calculated for several resistivities of the target layer (shaded area) and the parameters defined in Figure 7. These results assume that the casing conductance is unknown.

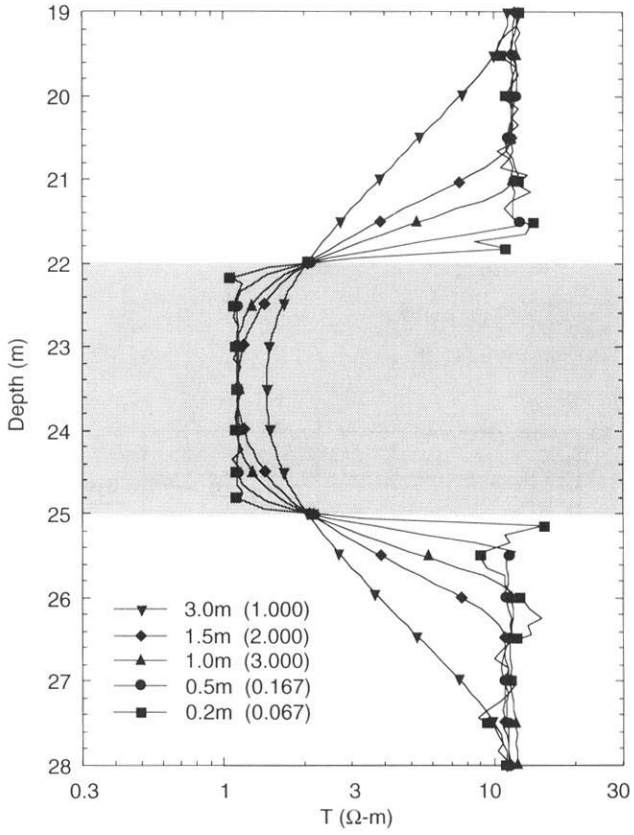

FIG. 10. The transverse resistance calculated using different electrode separations. The values in the parentheses are the electrode spacings normalized by the bed thickness (3 m).

at least to first order, it should have no sensitivity to the presence of uniform annular regions of varying conductivity. In this section, we will investigate the effects of an annular layer, which can represent a cement layer, on the transverse resistance (T) measurements. Kaufman (1990) determines T in the presence of an annular layer by assuming only a radial current distribution outside the casing and thus employs a series resistance calculation of T:

$$T_s = \rho_f + \frac{\rho_{ca} - \rho_f}{2\pi} \ln\left[\frac{\Delta t}{a_{ca}} + 1\right], \qquad (15)$$

where T_s is the series resistance calculation of T, $a_{,}$. is the inner radius, Δt is the thickness, and ρ_{ca} is the resistivity of the annulus and ρ_f is the resistivity of the host medium.

Figure II shows T_s compared to T, computed numerically, for selected electrode separation distances as a function of the annulus thickness for a conductive (5 $\Omega \cdot$ m) and resistive (20 $\Omega \cdot$ m) annulus. Although T is larger than $T_{,}$, the behavior of the resistances generally agrees with each other. For a thin annulus, the resistance approaches the background medium resistivity. As Δt increases, T asymptotes to the annulus resistivity. There are nearly no variations of T for a given thickness. This indicates that within the numerical accuracy, the radius of investigation is nearly independent of the electrode separation for a uniform annulus. Once again, departures from radial current Row are so small that effects from the parallel longitudinal resistances of annular layers are negligible. When the hole is cased, the combined resistivity measured in the presence of the annular layer cannot be distinguished from a formation that has an equivalent resistivity since modifying the electrode spacing does not change the radius of investigation.

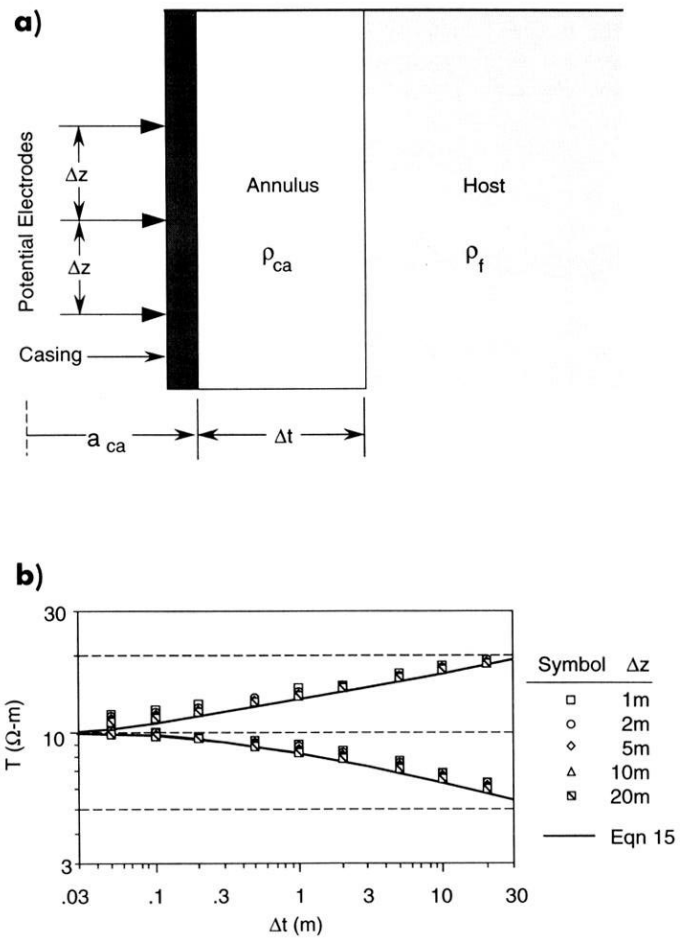

FIG. 11, Model of 50 m casing in a 10 $\Omega \cdot$ m host (a) used to calculate T_s, the series resistance, and T, *transverse* resistance, for several annular thicknesses (b). The transverse resistances are calculated for several electrode spacings and the center electrode is fixed at 2 m. The resistivities of the annulus are 5 $\Omega \cdot$ m and 20 $\Omega \cdot$ m.

The effects of thickness variations of the annulus in a homogeneous medium are illustrated in Figure 12. The model used for this simulation is a 50-m long casing surrounded by a 20 $\Omega \cdot$m annulus that has two thicknesses of 1.0 m and 0.2 m for the upper and lower section of the casing, respectively. Three resistivities of 1 $\Omega \cdot$m, 5 $\Omega \cdot$ m, and 10 $\Omega \cdot$m are used for the host formation. For low host resistivities, T agrees with T_s calculation to within 10 percent. As the host medium resistivity increases, the change of T *on* the thick side is less dramatic than the T_s calculations. These results are compatible with the effects of a finite casing length as shown in Figure 6. There is a small fluctuation in T *as* the array approaches the discontinuity from the thin side. This may be caused by the small distortion in radial flow as the step in the annulus is approached, but it seems unlikely that this could be detected in real data.

These analyses all show that at least to first order all the current flow in the formation adjacent to the casing is radial. The small longitudinal currents, which in fact explain why the computed values of T from equation (4) do not exactly equal the formation resistivity, are insignificant compared to the radial currents seen outside the casing.

Effects away from the borehole

On another scale, the currents that leave the casing radially can readily be distorted by features away from the borehole and can distort the measured potentials at some distance away from the hole. To illustrate this phenomena, we calculated the potentials along a vertical line (another uncased borehole) 100 m away from the cased hole with a current source I_0 (Figure 13). For this simulation, we substituted an annular disk of thickness 2 m and radii of 25 and 50 m for the layer that we studied previously for the TCRT™. In Figure 14, we show the results for an uncased well and the difference in potential with and without the disk expressed as a percentage of the field without the disk. In the second simulation, we calculated the same difference but with casing present. The effect of the conductive annulus is much greater for the cased hole. This result shows that crosswell resistivity measurements, using one cased well, are more sensitive to the parameters of the annular targets (such as steam injection zones) than measurements using uncased wells.

The explanation for this result lies in the analysis of the current vectors for each simulation as shown in Figure 15. In the uncased well, the conductive annulus simply keeps the current channeled in the annulus and increases the potential and decreases the "spread" in the adjacent well. For the

cased well, the current source is a distribution of radial currents which, without the annulus, yields a very broad potential field in the adjacent hole. The annulus "collects" this current and creates a larger and shaper potential distribution which, it turns out, is relatively greater than its uncased counterpart.

CONCLUSIONS

This numerical study of the through casing resistivity apparatus has demonstrated that the approximation used by Vail (1989a b) and Kaufman (1990) to determine the formation resistivity depends very much on the length of the casing and on the position of the measuring apparatus within the casing. Even in a casing that is effectively infinite (several times longer than its conduction length), there is enough longitudinal current outside the casing to cause significant errors in the estimation of formation resistivities for typical casing parameters. On the other hand, the resolution of a layer boundary, or the response to a layered annulus or to annuli of varying radii, is accurately described under the assumption of purely radial current flow. Thus the layer boundary resolution is set by the electrode separation and the measured resistance of a layered annulus, such as a cement layer or cement layer plus invasion zone, is simply described by the equivalent series resistance and is completely independent of the electrode spacing.

For typical casing conductances and formation resistivities, the approximate formulas for the formation resistivity have errors of up to 60 percent which, for many applications where relative changes between formations may be of interest, may be good enough. For more accurate estimates some iterative scheme will have to he developed where the casing parameters, casing length, and position of the measuring array within the casing are used in a process of refining the formation resistivity first estimated with the approximate formula.

This study has also shown that a cased well may he used very effectively in crosshole resistivity surveys. In this application, the radial currents from the cased hole produce greater relative distortions in the potentials in an adjacent uncased hole for a simple target than do the point source currents from an uncased well.

ACKNOWLEDGMENTS

This work was supported by the United States Environmental Protection Agency through Interagency Agreement Number DW89933758 to Lawrence Berkeley Laboratory and by ParaMagnetic Logging, Inc. and Gas Research Institute through contract number UCB Eng-7724.

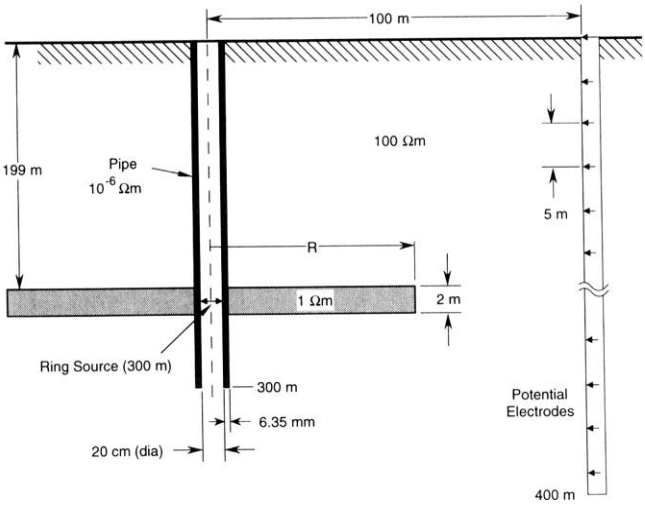

FIG. 13. Configuration for the crosshole resistivity monitoring simulation of an injection process.

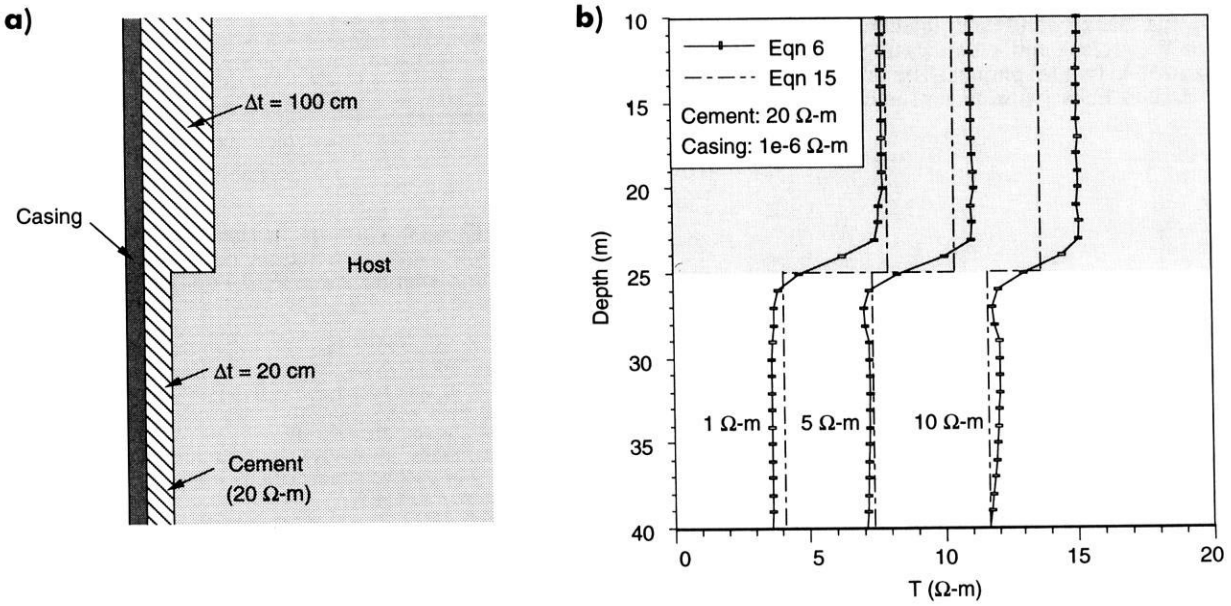

FIG. 12. Model configuration of cement annulus with variable thickness in an homogeneous host (a). Series resistance, T_s, (dashed line) and transverse resistance, T, (solid line) for a 1 $\Omega \cdot m$, 5 $\Omega \cdot m$, and 10 $\Omega \cdot m$ host medium (b).

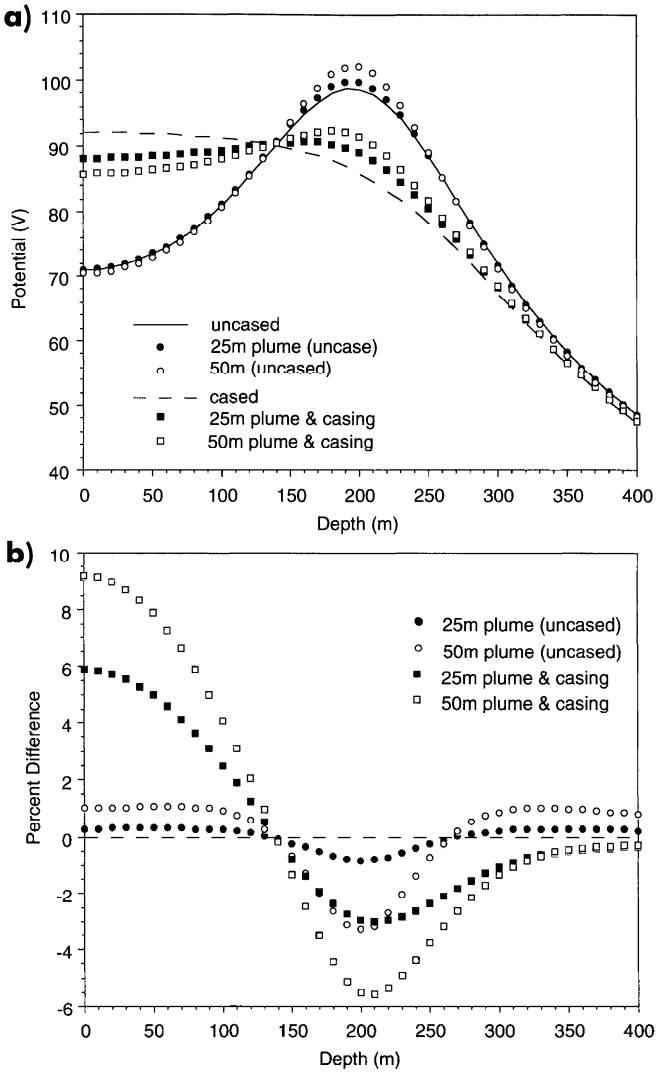

FIG. 14. Plots of the potentials (a) and percent difference between the background and injection potentials (b) for plume only (circles) and plume/casing (squares) for 25 m (black) and 50 m (white) plumes. The pre-injection potentials are the dashed lines (with casing) and solid lines (without casing).

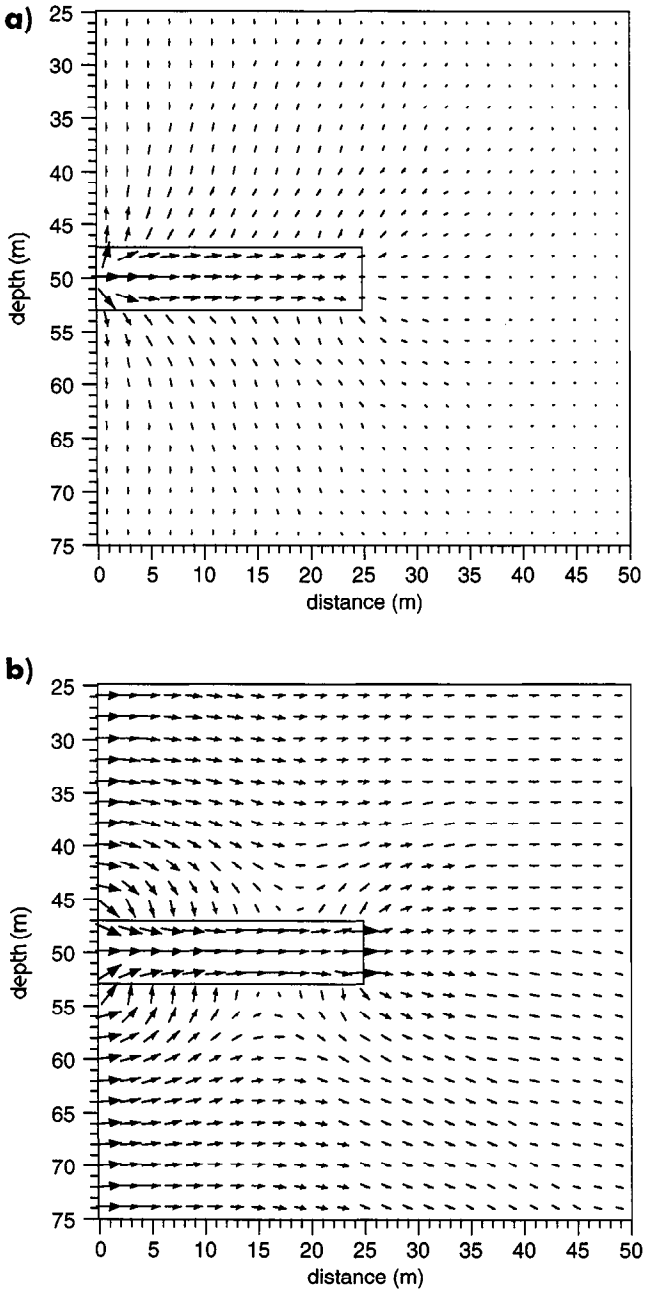

FIG. 15. Current patterns in the medium and conductive plume for the mise-a-la-masse, point source in an uncased hole, (a) and energized casing (b) configurations.

REFERENCES

Eloranta, E. H., 1986, Potential field on a stationary electric current using Fredholm's integral equations of the second kind: Geophys. Prosp., 34, 856-872.

Gard, M. F., Kingman, J. E. E., and Klein, J. D., 1989, Method and apparatus for measuring the electrical resistivity of geological formations through metal drill pipe or casing: U.S. patent 4,837,518.

Kaufman, A. A., 1989, Conductivity determination in a formation having a cased well: U.S. patent 4,796,186.

1990, The electric field in a borehole with a casing: Geophysics, 55, 29-38.

Luke, Y. L., 1962, Integrals of Bessel functions: McGraw-Hill Book co.

Schenkel, C. J., 1991, The electric resistivity method in cased boreholes: Ph.D. thesis, Univ. of California, Berkeley.

Schenkel, C. J., and Morrison, H. F., 1990, Effects of well casing on potential field measurements using downhole current sources: Geophys. Prosp., 38, 663-686.

Vail, W. B., 1989a, Methods and apparatus for measurement of the resistivity of geological formations from within cased boreholes: U.S. patent 4,820,989.

1989b, Methods and apparatus for measurement of electronic properties of geological formations through borehole casing: U.S. patent 4,882,542.

Vail, W. B., Momii, S. T., Woodhouse, R., Albertty, M., Peveraro, R. C. A., and Klein, J. D., 1993, Formation resistivity measurements through metal casing; Trans., SPWLA 34th Ann. Log. Symp.